DIAPH3 governs the cellular transition to the amoeboid tumour phenotype

Martin H. Hager[1,2†,‡], Samantha Morley[1,2‡], Diane R. Bielenberg[2,3], Sizhen Gao[4], Matteo Morello[1,2,5], Ilona N. Holcomb[6], Wennuan Liu[7], Ghassan Mouneimne[4], Francesca Demichelis[8,9], Jayoung Kim[1,2,5], Keith R. Solomon[1,10], Rosalyn M. Adam[1,2], William B. Isaacs[11], Henry N. Higgs[12], Robert L. Vessella[13], Dolores Di Vizio[1,2,5], Michael R. Freeman[1,2,5,14]*

Therapies for most malignancies are generally ineffective once metastasis occurs. While tumour cells migrate through tissues using diverse strategies, the signalling networks controlling such behaviours in human tumours are poorly understood. Here we define a role for the Diaphanous-related formin-3 (DIAPH3) as a non-canonical regulator of metastasis that restrains conversion to amoeboid cell behaviour in multiple cancer types. The *DIAPH3* locus is close to *RB1*, within a narrow consensus region of deletion on chromosome 13q in prostate, breast and hepatocellular carcinomas. DIAPH3 silencing in human carcinoma cells destabilized microtubules and induced defective endocytic trafficking, endosomal accumulation of EGFR, and hyperactivation of EGFR/MEK/ERK signalling. Silencing also evoked amoeboid properties, increased invasion and promoted metastasis in mice. In human tumours, DIAPH3 down-regulation was associated with aggressive or metastatic disease. DIAPH3-silenced cells were sensitive to MEK inhibition, but showed reduced sensitivity to EGFR inhibition. These findings have implications for understanding mechanisms of metastasis, and suggest that identifying patients with chromosomal deletions at *DIAPH3* may have prognostic value.

INTRODUCTION

Improving clinical options for metastatic disease requires an understanding of the molecular basis for the complex behaviours of metastatic cells. To date, however, few genetic lesions in human tumours that promote selection of metastatic variants have been identified.

Tumour cell migration can lead to metastatic dissemination. The ability of carcinoma cells to transition from an adherent, epithelial phenotype to a migratory, mesenchymal phenotype (the epithelial-to-mesenchymal transition, EMT) is well established, as are many signalling networks responsible for this transformation (Kalluri & Weinberg, 2009). However, it has recently been recognized that cancer cells can further transition

(1) Urological Diseases Research Center, Children's Hospital Boston, Boston, MA, USA
(2) Department of Surgery, Harvard Medical School, Boston, MA, USA
(3) Vascular Biology Program, Children's Hospital Boston, Boston, MA, USA
(4) Department of Cell Biology, Harvard Medical School, Boston, MA, USA
(5) Division of Cancer Biology and Therapeutics, Samuel Oschin Comprehensive Cancer Institute, Cedars-Sinai Medical Center, Los Angeles, CA, USA
(6) Department of Pathology, Stanford University School of Medicine, Stanford, CA, USA
(7) Center for Cancer Genomics, Wake Forest University, Winston-Salem, NC, USA
(8) Department of Pathology and Laboratory Medicine, Weill Cornell Medical College, New York, NY, USA
(9) Centre for Integrative Biology, University of Trento, Trento, Italy

(10) Department of Orthopaedic Surgery, Children's Hospital Boston, Harvard Medical School, Boston, MA, USA
(11) Department of Urology and Oncology, Johns Hopkins School of Medicine, Baltimore, MD, USA
(12) Department of Biochemistry, Dartmouth Medical School, Hanover, NH, USA
(13) Department of Urology, University of Washington, Seattle, WA, USA
(14) Department of Biological Chemistry and Molecular Pharmacology, Harvard Medical School, Boston, MA, USA

*Corresponding author: Tel: +1 310 423 7069; Fax: +1 310 423 0139;
E-mail: michael.freeman@cshs.org

† Present address: R&D Division, Oncology Research Laboratories, Daiichi Sankyo Europe, Munich, Germany
‡ These authors contributed equally to this work.

to an 'amoeboid' phenotype (called the mesenchymal-to-amoeboid transition, MAT), characterized by a rounded morphology, extensive actomyosin contractility, rapid extension and retraction of membrane protrusions (blebs), and reduced dependence on proteolysis for migration (Friedl & Wolf, 2010). Amoeboid cells are behaviourally plastic, move rapidly through extracellular matrices by deforming their shape, and express surface proteins more symmetrically than mesenchymal cells, thus facilitating opportunistic responses to changes in the microenvironment (Schmidt & Friedl, 2010). While such characteristics enable cells to readily migrate through extracellular matrix (ECM), the clinical impact of the amoeboid phenotype is unknown. Additionally, EMT (Kalluri & Weinberg, 2009) and MAT (Wolf et al, 2003) are reversible processes, and the ability of tumour cells to switch between these varied states presents challenges in defining critical signalling nodes where metastasis might be inhibited. While the amoeboid phenotype is potentially relevant to aggressive cancer (Sanz-Moreno & Marshall, 2010), it has not been well studied in human tumours.

Chromosome 13 is frequently altered in cancer, and the q-arm suffers predominantly from deletions (Beroukhim et al, 2010). The RB1 locus at 13q14.2 is thought to be the dominant tumour suppressor affected by copy number alterations. However, reports speculate that another tumour suppressor resides in this region, whose loss is associated with breast (Kainu et al, 2000) and invasive prostate (Dong et al, 2000) cancers, and whose restoration can inhibit metastatic dissemination (Hosoki et al, 2002).

Proximal to RB1, at 13q21.2, is the DIAPH3 locus encoding the protein Diaphanous-related formin-3 [DIAPH3, (Peng et al, 2003)]. This protein belongs to a family of formin orthologs (Chalkia et al, 2008) that nucleate, elongate and bundle linear actin filaments and regulate microtubule dynamics (Bartolini & Gundersen, 2010; Gaillard et al, 2011; Goode & Eck, 2007). Formins are required for such fundamental processes as endocytic trafficking, mitosis, cell polarity and migration (Goode & Eck, 2007). Despite the deregulation of these events in pathological states such as cancer, the role of DIAPH3 in disease is unexplored. We recently reported that genomic loss at DIAPH3 was linked to metastatic prostate cancer (Di Vizio et al, 2009). However, given the propensity for chromosomal loss along 13q in multiple cancers (Beroukhim et al, 2010), whether DIAPH3 deletions are driver or passenger lesions remained unresolved.

We now demonstrate that genomic loss at DIAPH3 is associated with multiple tumour types, and that DIAPH3 resides at an important signalling node that controls the amoeboid phenotype. We show that DIAPH3 silencing disrupts microtubules, impairs endocytosis and prevents EGFR downregulation, thereby enhancing EGFR activity and that of its downstream effectors MEK and ERK. DIAPH3 deficiency also promotes motility, invasion and experimental metastasis and significantly correlates with aggressive disease in human tumours.

RESULTS

Loss of DIAPH3 with tumour progression

To test whether genomic loss at DIAPH3 is a driver or passenger effect consequent to the general instability of chromosome 13q, we employed the genomic identification of significant targets in cancer (GISTIC) platform (Beroukhim et al, 2010). GISTIC identified regions of somatic copy number alterations (SCNA) in a pooled analysis of 26 different cancer types, most of which are not associated with previously validated tumour suppressor genes. We hypothesized that significant (q-value ≤ 0.25) focal SCNA harbouring a tumour suppressor would emerge as a consensus area across these cancers. Among the deletion peaks on chromosome 13, one containing three genes, protocadherin 17 (PCDH17), tudor domain-containing protein 3 (TDRD3) and DIAPH3, was located in a region common to three carcinomas (prostate, breast and hepatocellular, Fig 1A). DIAPH3, near the centre of this consensus region, was deleted in 32% of prostate, 46% of breast and 31% of hepatocellular carcinomas (Supporting Information Fig S1A). Together with the associated q-value range of $0.052 \leq q \leq 0.132$, these data suggest that DIAPH3 deletions are enriched by selective pressure. In support of this hypothesis, Oncomine expression profiles indicated DIAPH3 mRNA levels were lower in high stage prostate cancer (PCa) and in hepatocellular and invasive breast carcinomas than in normal tissue [Fig 1B–D; (Finak et al, 2008; Li et al, 2006; Mas et al, 2009)].

Given the prevalence of DIAPH3 lesions in multiple tumour types, we examined DIAPH3 status in metastases, using PCa as a representative disease model. Metastatic PCa lesions can originate from a single cell (Liu et al, 2009) and may lie dormant for many years (Wikman et al, 2008). For these reasons, we characterized the DIAPH3 status of disseminated tumour cells (DTCs) isolated from bone marrow of PCa patients (Holcomb et al, 2008). Deletions were more frequent in DTCs with either prostate-confined (31%) or metastatic (46%) disease

Figure 1. Genomic loss at DIAPH3 in invasive and metastatic tumours.

A. The DIAPH3 locus on chromosome 13q21.2 is located in a focal peak region of significant deletion ($q \leq 0.25$) common in prostate, hepatocellular and breast carcinomas. Only three genes, PCDH17, TDRD3 and DIAPH3, are focally deleted in all cancer subtypes.

B-D. DIAPH3 mRNA levels in prostate (PCa, stage T2/T3), hepatocellular and invasive breast carcinomas compared to normal tissue.

E. Frequency of loss at DIAPH3 (grey line) in DTCs aspirated from bone marrow of patients with prostate-confined cancer ($n = 48$, blue) and advanced PCa ($n = 11$, red). Determined by array CGH and compared to copy number status in the primary tumours ($n = 9$, green). The chromosome band for each genomic position is shown; tick marks above indicate gene locations on chromosome 13.

F. DIAPH3 copy number status grouped by Gleason score and compared with metastases.

G. DIAPH3 copy number analysis in matched primary tumours and metastases (Met) reveals significant loss in metastatic disease.

H. DIAPH3 gene copy number in PCa samples grouped by Gleason Score in comparison to metastases (Met).
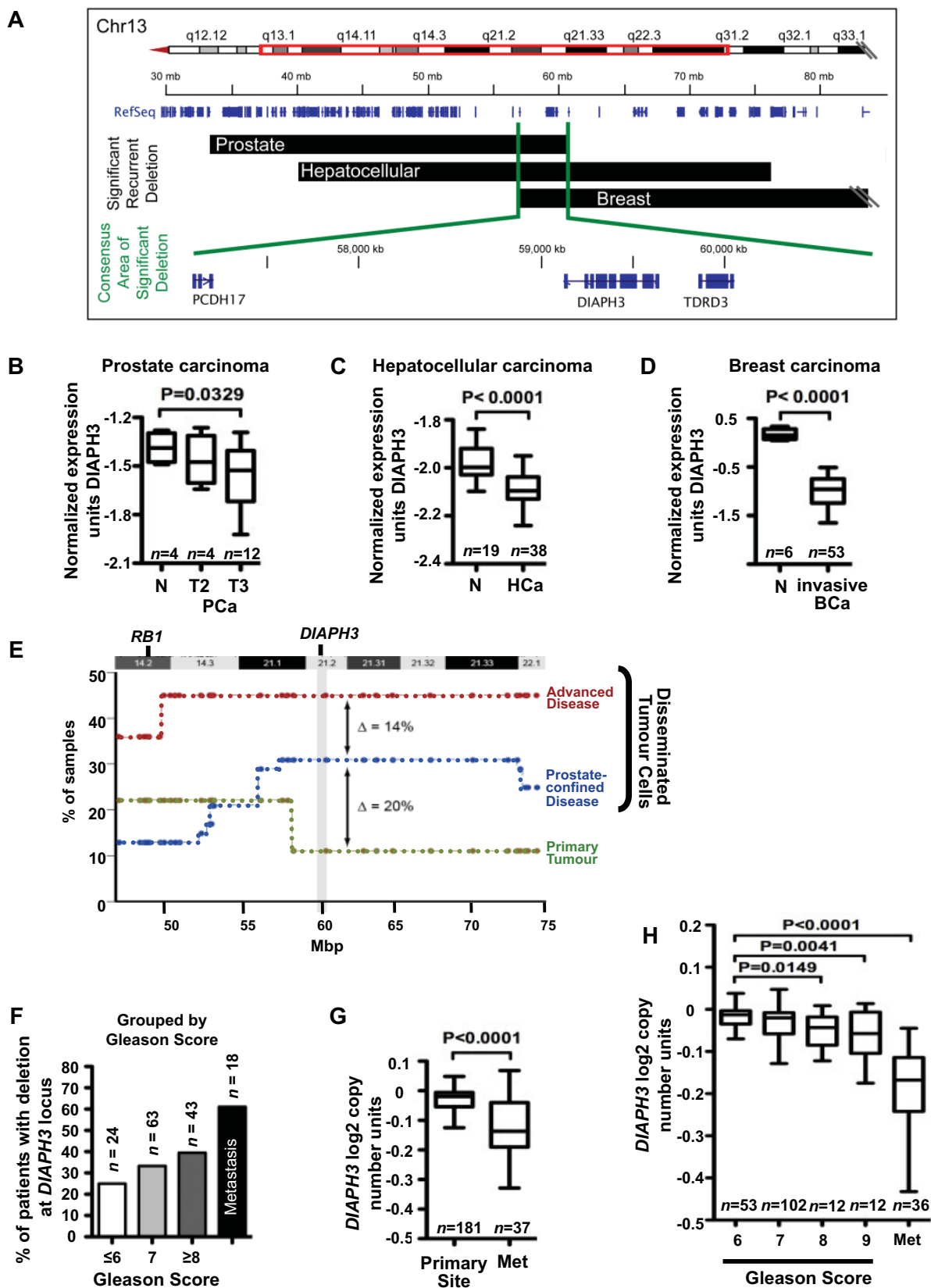
Figure 1.

than in primary tumours (10%, Fig 1E), suggesting that *DIAPH3* loss is related to dissemination from the primary site.

To examine this possibility, we evaluated *DIAPH3* copy number in primary tumours and metastases of 148 prostate cancers by Affymetrix Genome-Wide Human SNP Array 6.0 (Liu et al, 2009). Loss at *DIAPH3* was increasingly prevalent with progression, occurring in 25% of low grade (Gleason score ≤6), 33% of intermediate grade (Gleason score 7), 40% of high grade (Gleason score ≥8), and 61% of metastatic tumours (Fig 1F, Supporting Information Fig S1B). Oncomine copy number data confirmed *DIAPH3* genomic loss and its significant correlation with disease progression, which increased from primary tumour to metastatic lesions and with increasing Gleason score [Fig 1G and H; (Taylor et al, 2010)].

DIAPH3 knockdown induces an amoeboid phenotype in transformed cells

In order to examine the biological consequences of *DIAPH3* loss, we employed RNAi against DIAPH3 with multiple independent shRNAs or siRNAs (Supporting Information Fig S2A, Fig 6C), which efficiently reduced DIAPH3 protein levels but did not affect the related proteins DIAPH1 and DIAPH2 (Supporting Information Fig S2B). Because *DIAPH3* loss was observed in breast cancers (Fig 1A and D), we employed the disease-relevant human mammary epithelial cell (HMEC) model. While stable DIAPH3 knockdown did not alter HMEC cell morphology in 2D culture, it modestly enhanced proliferation (Fig 2A, Supporting Information Fig S2C and D). In reconstituted basement membrane gels (3D culture), DIAPH3 silencing induced enlarged acinar structures with aberrant architecture and distribution of Laminin V (Fig 2A, Supporting Information Fig S3A and B), resembling that seen with ErbB2 activation (Debnath et al, 2002). These results suggest that in normal epithelia, DIAPH3 may act to suppress oncogenic behaviour.

Next, we investigated the consequences of DIAPH3 loss in the context of HRAS-induced cellular transformation. We generated stable populations of HRAS^{V12}-transformed HMECs in which DIAPH3 was silenced (Supporting Information Fig S3C). In 2D culture, HMEC-HRAS^{V12} cells appeared spindle-shaped, consistent with EMT (Fig 2B, *top*). In contrast, DIAPH3-depleted HMEC-HRAS^{V12} cells were refractile, with rounded morphologies (Fig 2B). Time-lapse video microscopy demonstrated that these cells displayed abundant, reversible eruption of blebs, reduced cell–cell contact, and increased rates of random

motility, in comparison to HMEC-HRAS^{V12} cells (Fig 2C and D, Supporting Information Movies S1, S2). These features are indicative of amoeboid behaviour (Wolf et al, 2003).

In 3D culture, HMEC-HRAS^{V12} produced large cell aggregates (acini) with penetration of the matrix by cords of spindle-shaped cells (Fig 2B, *top inset*, Supporting Information Fig S3D). In contrast, DIAPH3-deficient HRAS^{V12} cells produced acini that progressively and dramatically lost structural integrity, coinciding with extensive migration of round cells into the matrix (Fig 2B, *lower insets*, Supporting Information Fig S3D). Significantly, while HRAS^{V12}-HMEC cells were poorly invasive through collagen I, DIAPH3 knockdown in this cell background promoted invasion (Fig 2E). These findings indicate that, when combined with activated HRAS, DIAPH3 down-regulation promotes an amoeboid phenotype and increases invasion.

To determine whether this amoeboid transition can be similarly induced in genuine cancer cells, we silenced DIAPH3 in DU145 PCa cells. As in the genetically defined HRAS^{V12}-HMEC model, DIAPH3 knockdown in DU145 cells induced a rounded morphology and formation of membrane blebs when cells were embedded in collagen (Fig 2F). In line with this promotion of amoeboid behaviour (Fig 2G), DIAPH3 knockdown enhanced the invasiveness of DU145 cells (Fig 2H, Supporting Information Fig S3E). DIAPH3-deficient cells were hypersensitive to chemo-attractants, including EGF.

Amoeboid cells display weakened substrate adhesions, allowing high cell velocities (Schmidt & Friedl, 2010). This fast 'gliding' mode can be driven by Rho-kinase (ROCK)-dependent force generation through myosin light chain (MLC2) phosphorylation, and is distinct from integrin-mediated traction force generation characteristic of mesenchymal motility (Friedl & Wolf, 2010). DIAPH3 silencing promoted focal adhesion disassembly, as evidenced by an altered pattern of focal adhesion kinase (FAK) phosphorylation [Fig 3A, 3B (Hamadi et al, 2005)], and also evoked high levels of phosphorylated MYPT1, a ROCK substrate (Fig 3C and D), and MLC2 (Fig 3E). In DIAPH3-deficient cells, both activated and total MLC2 were enriched at the cell cortex (Fig 3F, Supporting Information Fig S4A–C), where cortical MLC2 colocalized with phalloidin. In unsilenced cells, cortical MLC2 was less pronounced and co-localized instead with phalloidin in stress fibres. These findings are consistent with the ROCK-mediated cortical localization of MLC2 reported to be displayed by amoeboid cells (Pinner & Sahai, 2008; Sahai & Marshall, 2003; Wyckoff et al, 2006).

Figure 2. DIAPH3 knockdown induces an amoeboid phenotype in transformed cells. ▶

A. Morphology of DIAPH3-depleted HMEC, compared to control cells. Plastic (2D), basement membrane cultures (3D). Scale = 200 µm.

B. HRAS^{V12} cells grown in 2D adopt a round, refractile appearance when DIAPH3 is silenced. Scale = 100 µm. HMEC-HRAS^{V12} cells form cell aggregates with cord-like protrusions in 3D. DIAPH3 depletion causes junctional instability, with migration of single cells into the surrounding matrix (*inset, right*). Scale = 200 µm.

C. Representative trajectories of control (green) and DIAPH3-deficient (red) HMEC-HRAS^{V12} cells.

D. Quantification of migration speed, determined from **C**.

E. DIAPH3-silenced HRAS^{V12}-HMEC display increased invasiveness.

F. Growth of DIAPH3-deficient and control DU145 cells on a thick layer of collagen I. Arrowheads mark cell surface blebbing (top). Visualization of the cytoskeleton with phalloidin by immunofluorescence (IF) shows prominent cortical actin in DIAPH3-deficient cells (arrowhead, bottom). Scale = 50 µm.

G. Increase in amoeboid morphology following expression of DIAPH3 siRNA.

H. Invasion of collagen I by DU145 cells, with FBS or EGF as chemo-attractants, is increased in DIAPH3-deficient cells ($N \geq 2$ independent trials). See also Supporting Information Movies S1 and S2.
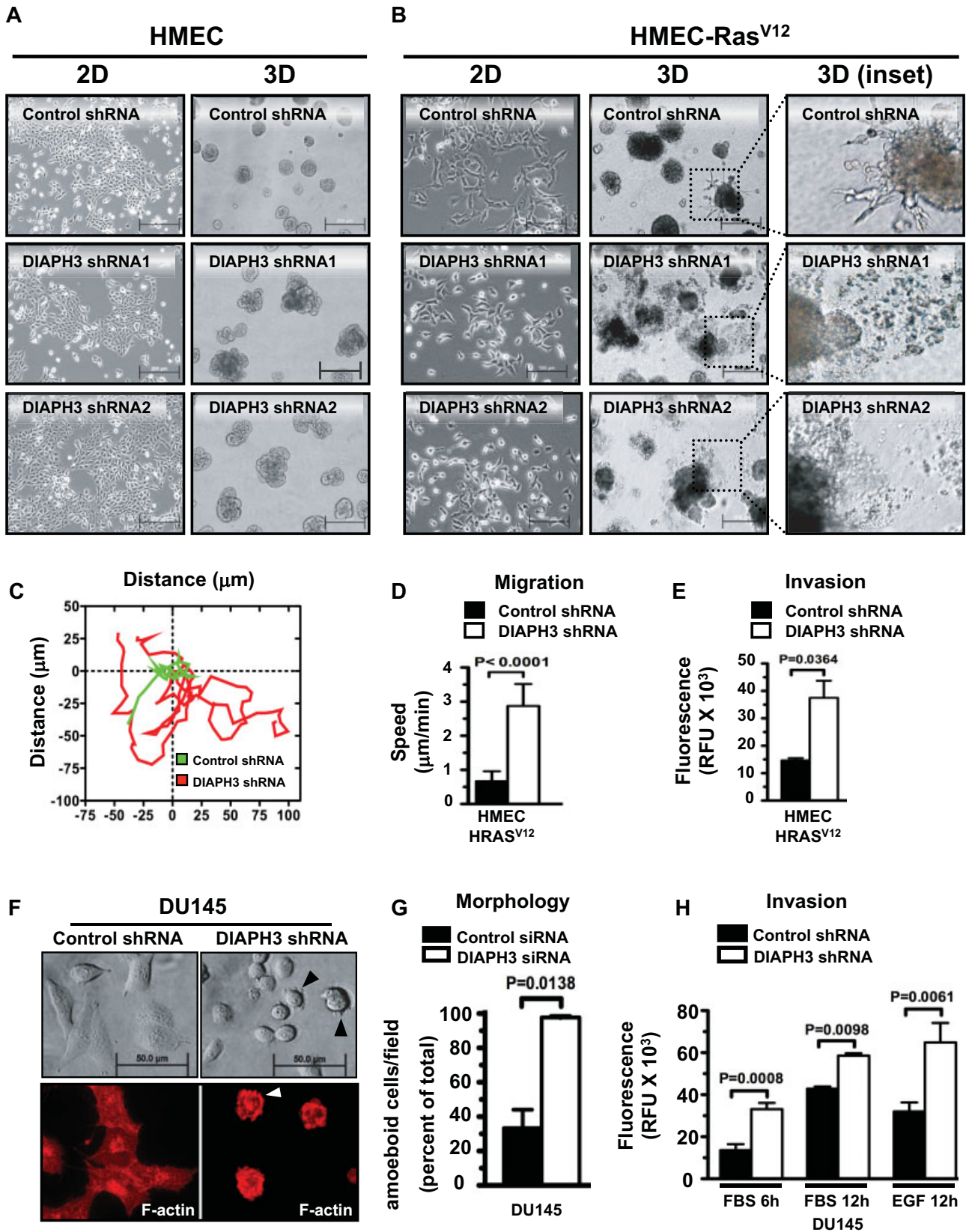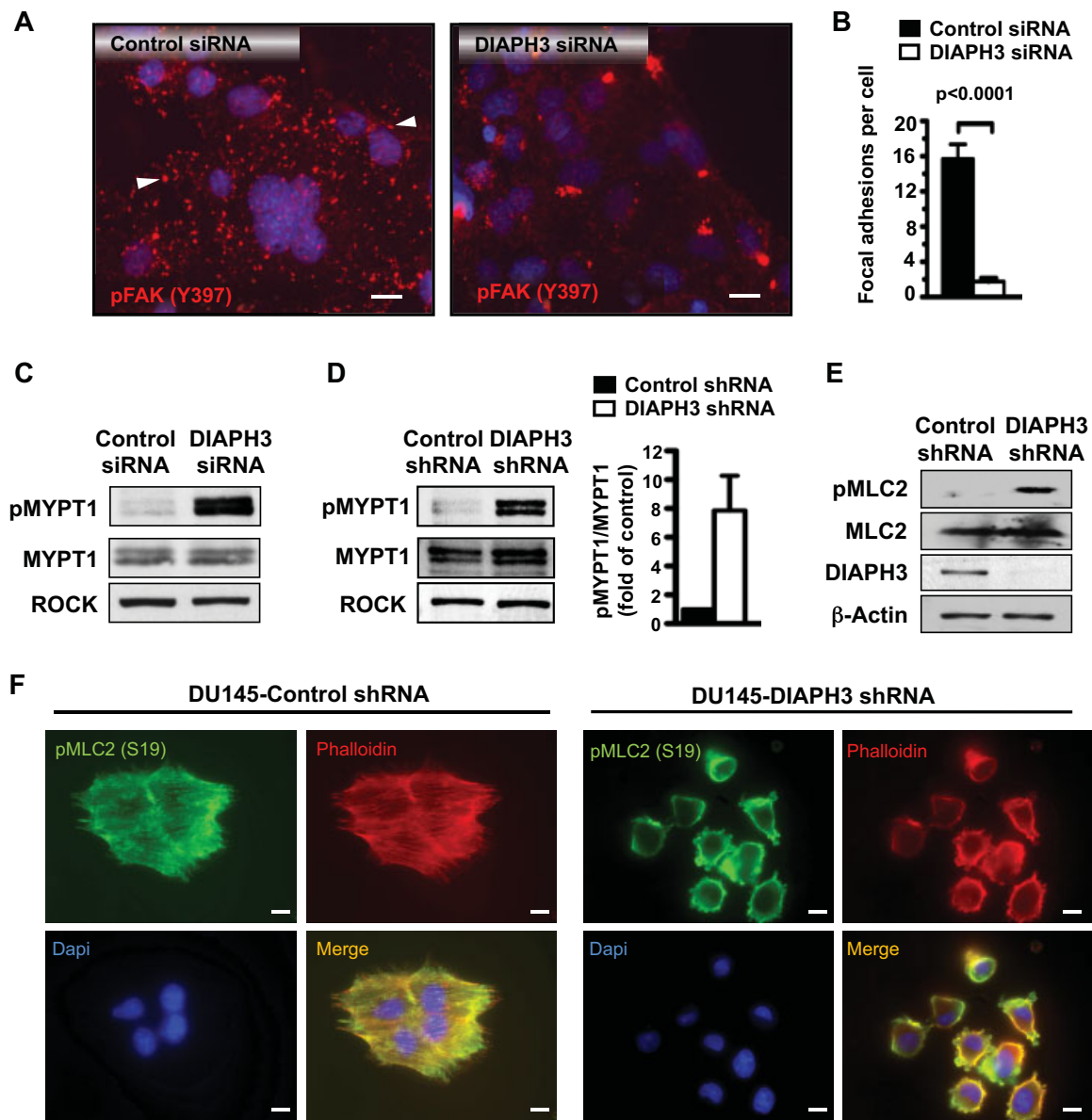
Figure 2.

Figure 3. DIAPH3 knockdown promotes biochemical features of the amoeboid transition.

A. The distribution of focal adhesions in COS7 cells, detected by IF with a phospho-FAK(Y397) antibody, is reduced in DIAPH3-deficient cells. Scale = 20 μm.

B. Quantitation of focal adhesions in **A**.

C-E. Enhanced phosphorylation of MYPT1 (**C,D**) and MLC2 (**E**) in DIAPH3-deficient DU145 cells indicates high ROCK activity.

F. Distribution of active (phosphorylated) MLC2 and F-actin (phalloidin) in DU145 stable lines. Scale = 10 μm ($N \geq 2$ independent trials).

DIAPH3 regulates EGFR trafficking and microtubule stability

We next sought to examine the mechanisms underlying induction of the amoeboid transition by DIAPH3 knockdown. Formins localize to endosomes and regulate vesicular trafficking (Fernandez-Borja et al, 2005; Gasman et al, 2003; Wallar et al, 2007). Because endocytosis governs the spatiotemporal regulation of receptor tyrosine kinases (RTKs), and chemotactic sensitivity to EGF was enhanced in DIAPH3-silenced cells (Fig 2H), we hypothesized that DIAPH3 may regulate turnover and trafficking of EGFR. Enforced expression of DIAPH3 markedly accelerated the kinetics of EGFR turnover and receptor inactivation in response to EGF and under steady-state conditions (Fig 4A, 4B). Further supporting a functional relationship, DIAPH3 and EGFR co-localized in endosomes (unpublished observations). Thus, we examined the influence of DIAPH3 on endocytic trafficking of EGFR. In the absence of EGF and the presence of endogenous DIAPH3, EGFR co-localized at the plasma membrane with the recycling marker Rab11 (Fig 4C). In response to ligand, EGFR translocated to a peri-nuclear region and co-localized with the early endosome marker Rab5 (Fig 4D). In contrast, DIAPH3 silencing promoted association of EGFR with endosomes enriched in Rab11, Rab5

and EEA1 (Fig 4C–E), even in absence of ligand. These findings suggest that loss of DIAPH3 disrupts vesicular transport, leading to EGFR accumulation in endosomes.

To investigate how DIAPH3 affects endosomal trafficking of EGFR, we assessed its influence on the actin and microtubule (MT) cytoskeletons, which govern short- and long-range vesicular transport, respectively (Soldati & Schliwa, 2006). While rearrangement of the actin cytoskeleton was associated with DIAPH3 silencing (Fig 3F, Supporting Information Fig S4C), no conspicuous actin defects were detected. Combined with the observation that endosomes did not accumulate at the cell cortex but were dispersed throughout the cytoplasm in DIAPH3-deficient cells (Fig 4C–E), these data suggest that DIAPH3 loss does not significantly influence short-range EGFR trafficking.

In addition to regulating actin dynamics, formins also promote MT stability (Bartolini et al, 2008). Enforced DIAPH3 markedly increased tubulin acetylation (Fig 5A, Supporting Information Fig S5A), an indication of MT stabilization (Verhey & Gaertig, 2007). Conversely, DIAPH3 silencing decreased tubulin acetylation and was associated with MT fragmentation (Fig 5B–G, Supporting Information Fig S5B). Notably, treatment of cells with the MT depolymerizing agent nocodazole phenocopied the accumulation of EGFR in internal vesicles and some amoeboid features (Supporting Information Fig S5C and D) induced by DIAPH3 knockdown.

These findings imply that DIAPH3 deficiency disrupts MT stability and endosome processing, thereby sequestering and preserving EGFR in early endosomes. Disrupted trafficking coincided with EGFR hyper-activation, as evidenced by increased auto-phosphorylation of activating residues and decreased phosphorylation of the inhibitory Thr669 site (Fig 6A). EGFR activation was enhanced in DIAPH3-silenced cells in response to EGF (Supporting Information Fig S6A). DIAPH3 deficiency also increased phosphorylation of the EGFR effectors MEK and ERK (Fig 6A and B, Supporting Information Fig S6A), which inversely and dose-dependently correlated with DIAPH3 levels (Fig 6C, Supporting Information Fig S6B). Even under serum-free conditions, DIAPH3 depletion increased ERK phosphorylation sixfold (Fig 6D), and potentiated the response to EGF (Fig 6E, Supporting Information Fig S6C), with a twofold to fourfold increase in phosphorylated ERK at each time point post-stimulation. This ligand-independent hyperactivation of EGFR and MEK/ERK is consistent with reports linking early endosome-localized EGFR to sustained activation of the RAF/MEK/ERK pathway (Sorkin & von Zastrow, 2009). Collectively,

these findings support an important role for DIAPH3 in regulation of EGFR trafficking and signalling.

Sensitivity of DIAPH3-deficient cells to anti-neoplastic agents

Because DIAPH3 silencing induces amoeboid behaviour and strongly activates ERK, we tested the relevance of MEK/ERK signalling in this scenario. Treatment of DIAPH3-deficient DU145, HMEC-HRAS^{V12} and A375P melanoma cells with the MEK1/2 inhibitor PD98059 converted cells to a more mesenchymal morphology (Fig 7A, Supporting Information Fig S7A). Pharmacologic reversion of amoeboid features could be reversed by drug washout (unpublished observations). A375P has been used as a model to study amoeboid properties (Sanz-Moreno et al, 2008). Collectively, these data indicate that MEK/ERK pathway activation can contribute to amoeboid behaviour in diverse cell backgrounds.

EGFR is a frequent target for therapeutic intervention. However, responsiveness to tyrosine kinase inhibitors (TKI, *e.g.* gefitinib) may be dictated by the receptor's subcellular localization (Huang et al, 2009). Because DIAPH3 knockdown modulates EGFR localization and activity, we asked whether DIAPH3 deficiency affects TKI sensitivity. In control DU145 cells, EGF stimulation induced amoeboid features (blebbing), which was suppressed by gefitinib (Fig 7B and C, Supporting Information Movie S3). In contrast, the amoeboid phenotype was constitutive and ligand-independent in DIAPH3-silenced cells. Notably, these cells were unresponsive to the TKI. These findings suggest that *DIAPH3* loss alters sensitivity to EGFR inhibitors.

Taxanes such as paclitaxel and docetaxel are first-line chemotherapies for metastatic breast and prostate cancers, which we show are prone to *DIAPH3* loss (Fig 1). However, development of resistance limits their efficacy in patients. Taxanes stabilize MTs, suggesting their potential to down-regulate EGFR similarly to DIAPH3. We observed, however, that EGFR activation persisted in the presence of docetaxel (Supporting Information Fig S7B) and paclitaxel (unpublished observations), in line with reports that these agents disrupt endosomal EGFR trafficking (Sonee et al, 1998).

DIAPH3 suppresses the amoeboid phenotype

Induction of the amoeboid phenotype by DIAPH3 knockdown suggests that enforced DIAPH3 expression may counteract this transition. We stably expressed GFP-DIAPH3 in PC3 PCa cells and in U87 glioblastoma cells. Of note, U87 expressed the lowest levels of DIAPH3 among the cell lines we tested. U87 and PC3

Figure 4. DIAPH3 regulates endocytic trafficking of EGFR.

A. Enforced DIAPH3 accelerates EGFR turnover. COS7 cells expressing empty vector (Vo) or DIAPH3 were serum-depleted overnight, treated with EGF for the indicated times, and lysates blotted with the antibodies shown.

B. GFP-DIAPH3-positive COS7 cells show strongly reduced EGFR levels (lower panel, arrowhead) in comparison with GFP-transfected control cells (upper panel) or adjacent untransfected cells. Scale = 20 μm.

C. *Left*, Co-localization of Cy3-labeled EGFR with FITC-labelled Rab11 in DU145 cells expressing DIAPH3 siRNAs. *Right*, Cell peripheries are shown in grey, and areas of co-localization in black. Insets show predominance of EGFR at the plasma membrane (top) or in endosomes (bottom). Scale = 20 μm.

D. *Left*, Co-localization of Cy3-labeled EGFR with FITC-labelled Rab5 upon ligand binding (+EGF). DIAPH3 loss evokes an increase in EGFR internalization in the absence of ligand (−EGF), as shown by accumulation in endosomes (insets and arrowheads) and co-localization with Rab5. Scale = 20 μm. *Right*, Quantitation of EGFR-enriched endosomes.

E. Cy3-labeled EGFR, which is localized at the plasma membrane in DU145 cells expressing control siRNA, is internalized and co-localizes with the FITC-labelled early endosome marker EEA1 in DU145 cells expressing DIAPH3 siRNAs. Scale = 10 μm (N ≥ 2 independent trials).
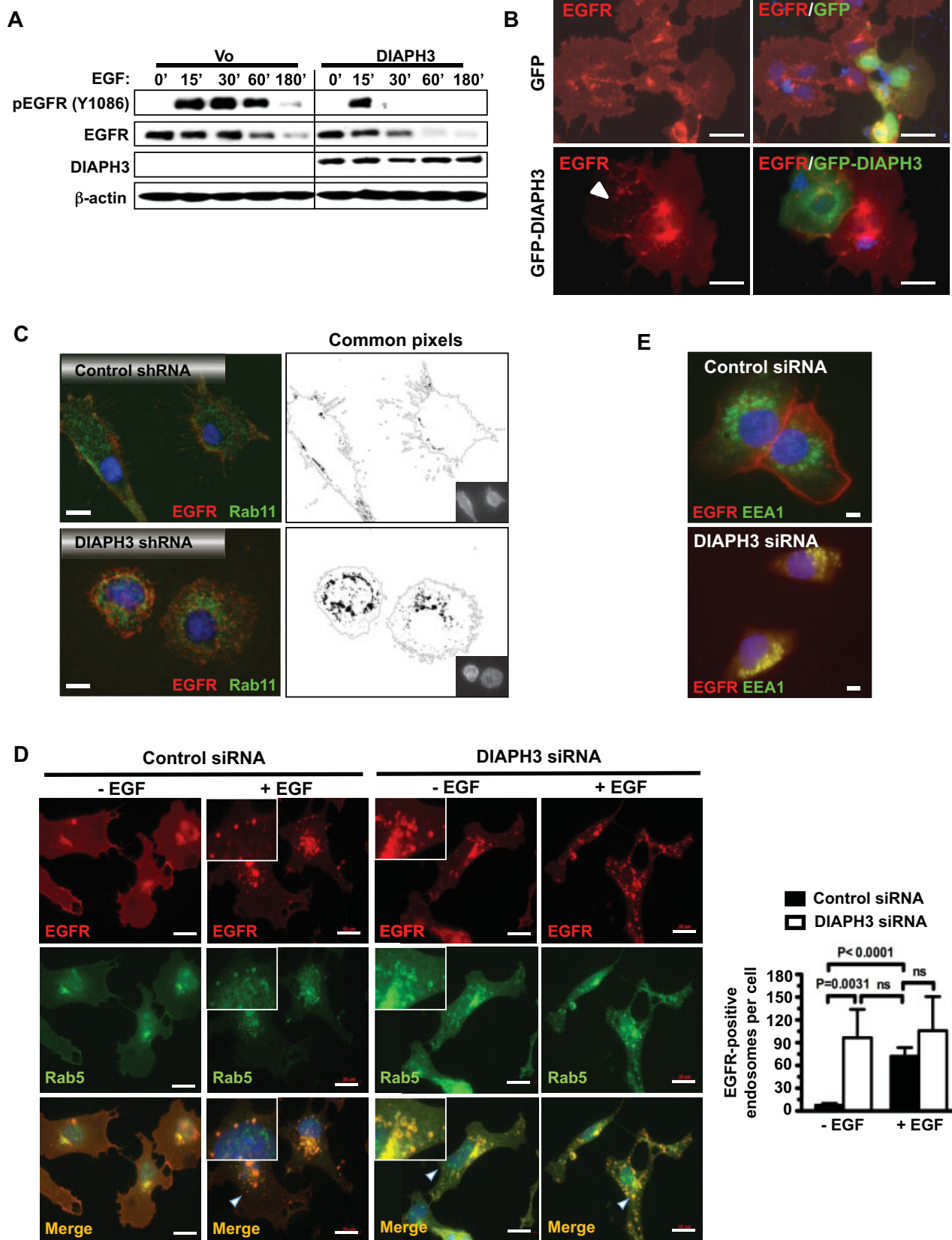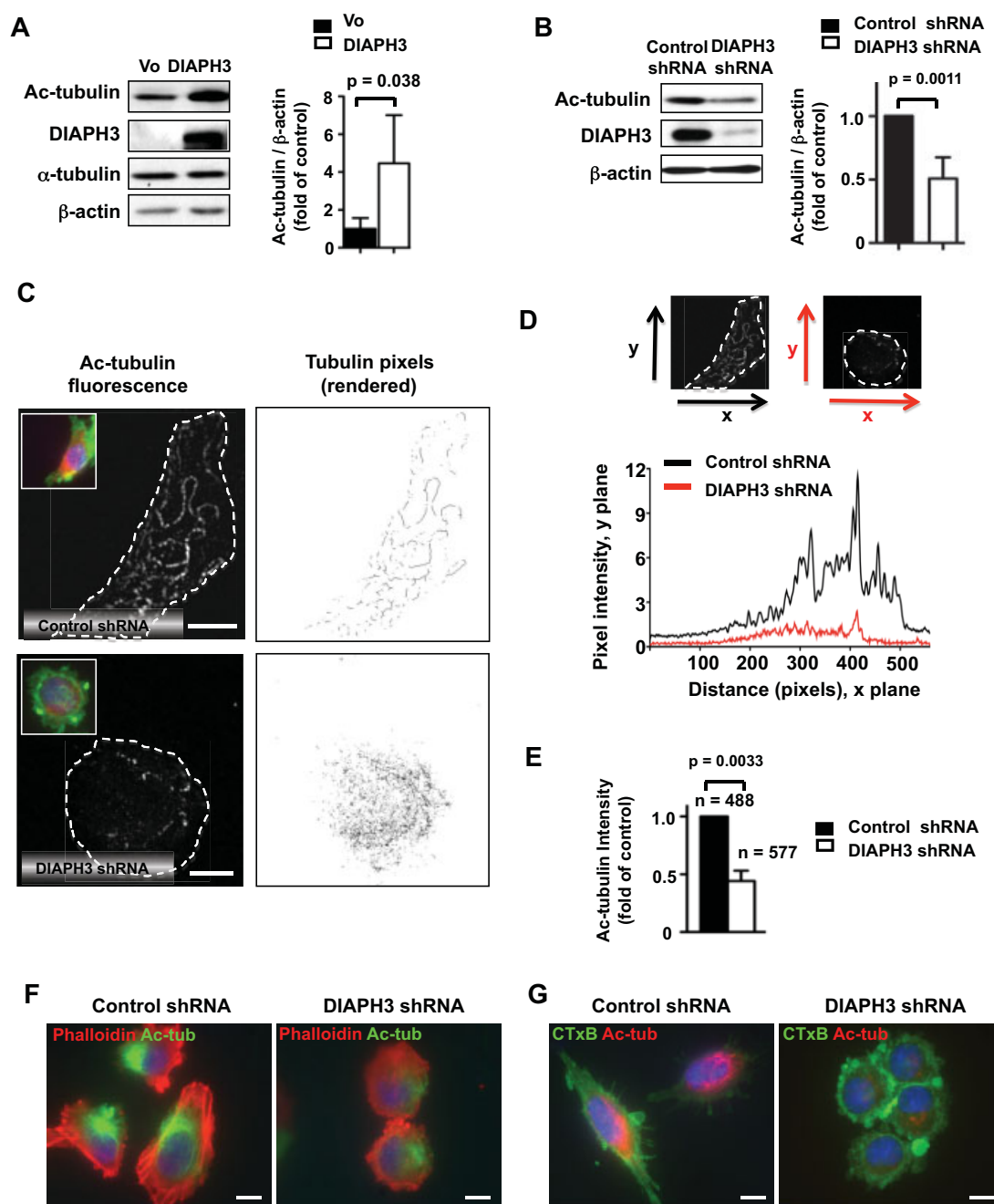
Figure 4.

Figure 5. DIAPH3 regulates microtubule topology and stability.

A. Increased acetylated tubulin (Ac-tubulin) in PC3 cells stably expressing DIAPH3.

B. Reduced Ac-tubulin levels in DU145 cells silenced for DIAPH3.

C. *Left*, Ac-tubulin IF showing MT fragmentation in DIAPH3-deficient DU145 cells grown in 3D. *Right*, MT topology was rendered by ImageJ. *Insets*, cells stained with cholera toxin B (CTxB, green). Scale = 10 μm.

D. Pixel intensity of **C** was quantified as a 2D contour plot, as a function of intensity in the *x versus y* planes (illustrated schematically, *top*).

E. The pixel intensity of Ac-tubulin was quantified in silenced or unsilenced DU145 cells. Cell peripheries were outlined as in **C**, tubulin intensity integrated within the enclosed area, and average intensities in each condition determined. Average intensity values determined from three independent trials (Student's *t*-test, $p = 0.0033$). $N =$ total cell number.

F,G. DU145 cells expressing control or DIAPH3 shRNAs were stained with Ac-tubulin following staining with rhodamine-phalloidin (**F**) or FITC-CTxB (**G**), and imaged by fluorescence microscopy. Scale = 10 μm ($N \geq 2$ independent trials).
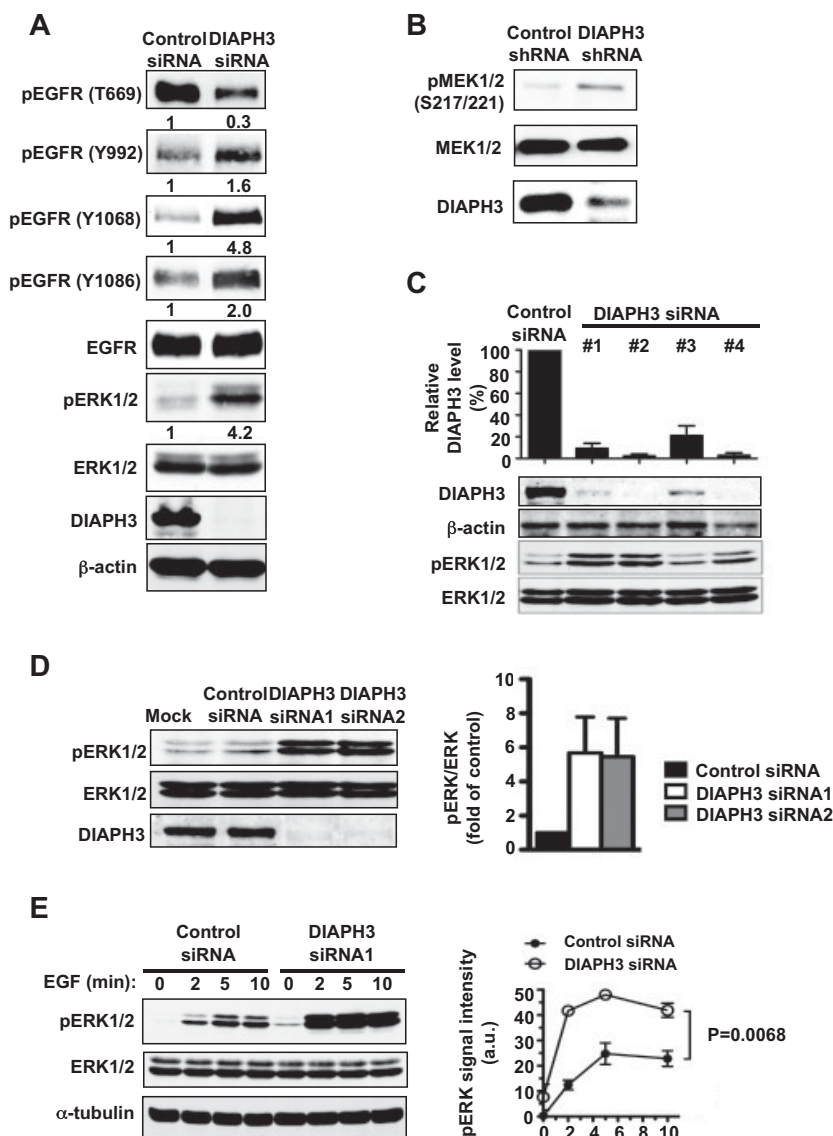
Figure 6. DIAPH3 knockdown enhances EGFR signalling.

A. EGFR is active in DIAPH3-silenced COS7 cells, as shown by increased tyrosine phosphorylation at activating sites and decreased phosphorylation of the T669 inhibitory site.

B. Enhanced pMEK1/2 in DIAPH3-depleted DU145 cells.

C. Targeting of DIAPH3 with four independent siRNAs in COS7 leads to >90% depletion, which inversely correlates with pERK1/2 levels.

D. DIAPH3 depletion in serum-depleted cells enhances pERK1/2 levels.

E. Acute, sustained phosphorylation of ERK1/2 in response to EGF in DIAPH3-depleted versus control cells (two-way ANOVA, $p = 0.0068$; $N \geq 2$ independent trials).

both were phenotypically amoeboid, with numerous membrane blebs and rounded morphologies (Fig 8A and B, Supporting Information Fig S8A). Enforced DIAPH3 altered the phenotype of both cell lines, suppressing amoeboid blebbing and inducing formation of prominent lamellipodia, a typical mesenchymal feature (Fig 8A, B and F, Supporting Information Fig S8A). DIAPH3 also increased levels of the mesenchymal marker N-cadherin (Fig 8C), in concert with increased stress fiber formation (Fig 8E, Supporting Information Fig S8B), suggesting that DIAPH3 promotes an amoeboid to mesenchymal transition.

The data shown above position DIAPH3 within the EGFR pathway. Consistent with this, we identified an EGF-sensitive phospho-serine at position 624 in the DIAPH3 primary sequence by tandem mass spectrometry (Supporting Information Fig S9A). S624 is located within the last of five polyproline/SRC homology three binding motifs in the FH1 domain (Fig 8D). This site was validated by stable isotope labelling (Supporting

Information Fig S9B and C) and confirmed to be EGF-responsive using a custom phosphosite-specific antibody (Supporting Information Fig S9D and E). DIAPH3 function was modulated by its phosphorylation status at S624. A phospho-null mutant at this site (S624A) promoted stress fibre formation, a mesenchymal characteristic (Fig 8E), and suppressed amoeboid blebbing (Fig 8F) to a greater degree than the unmodified protein, while a phospho-mimetic mutant (S624E) was impaired in both activities (Fig 8E and F). These findings support the conclusion that DIAPH3 suppresses amoeboid blebbing and is functionally inhibited by phosphorylation at S624, which occurs in response to EGF treatment (Supporting Information Fig S9E).

DIAPH3 loss promotes metastasis and is associated with metastatic human prostate cancer

Our findings thus far suggest that DIAPH3 loss promotes motility, invasion, and increased oncogenic signalling, all pre-requisites for
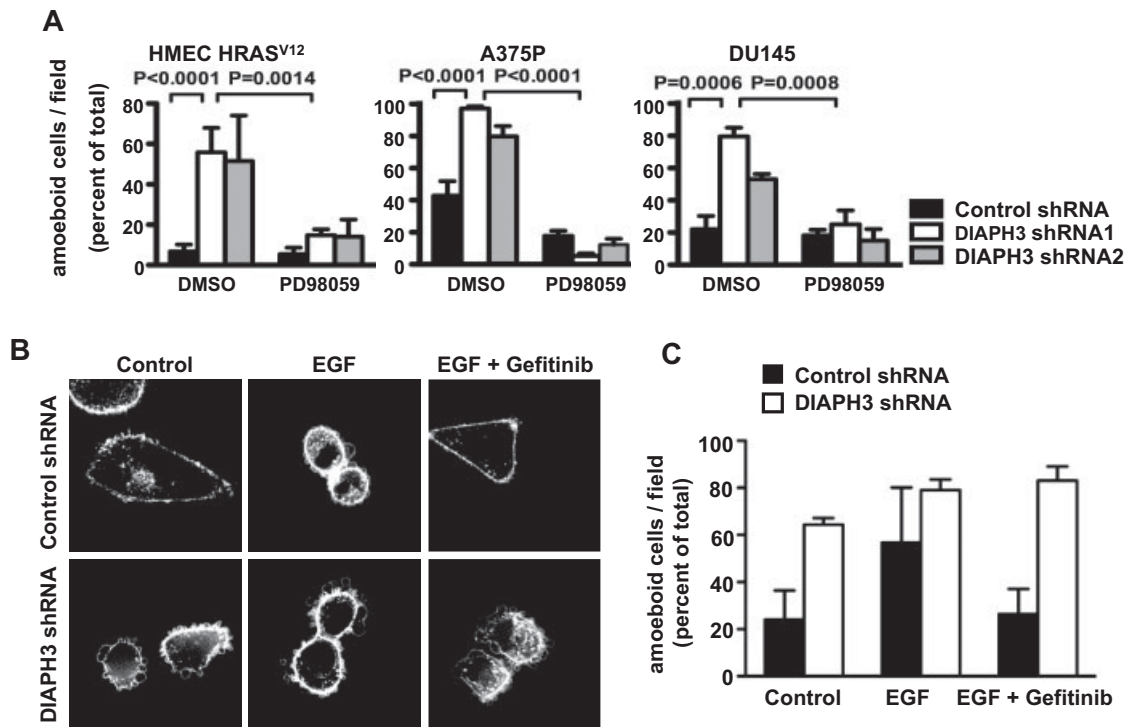
Figure 7. Sensitivity of amoeboid features to MEK1/2 and EGFR inhibition.

A. Amoeboid features induced by DIAPH3 silencing in human HMEC-HRAS[V12], A375P melanoma and DU145 cells can be reverted by PD98059 (50 μM). $N \geq 2$ independent trials.

B,C. Amoeboid blebbing induced by EGF (10 nM) in control cells is sensitive to the EGFR inhibitor Gefitinib (2 μM), while induction by DIAPH3 silencing is less sensitive to both treatments, (**C**) Representative micrographs, (**B**) See also Supporting Information Movie S3.

metastasis. Consistent with this hypothesis, superficial pulmonary metastases in nude mice, induced by tail vein injection of DIAPH3-silenced DU145 cells, were enhanced relative to unsilenced cells (Fig 9A and B). Both the number and size of metastatic foci were potentiated by DIAPH3 knockdown (Fig 9B and data not shown). Additionally, large tumour thrombotic emboli were observed only in lung sections from mice that underwent injection of DIAPH3-silenced cells (Fig 9C). Detection of human cytokeratin 18 (CK18) in the lung metastases demonstrated the lesions' human origin (Fig 9D). This was further confirmed by puromycin resistance of cells from dissociated lesions in cell culture. Together, these findings indicate that DIAPH3 silencing enhances experimental metastasis in mice.

Lastly, we examined expression of the DIAPH3 protein with PCa progression using a cohort of 90 human prostate specimens in a tissue microarray format and a validated anti-DIAPH3 antibody (Supporting Information Fig S2B). While DIAPH3 protein levels did not demonstrably change between benign and organ-confined carcinoma, we observed a dramatic reduction of DIAPH3 protein levels in metastatic lesions in comparison with normal tissue ($p = 0.018$) and organ-confined tumours ($p = 0.007$, Fig 9E and F). These results are in agreement with our genomic analyses (Fig 1E–H) and indicate that loss of the DIAPH3 locus functionally results in significant loss of the protein in human metastatic disease.

DISCUSSION

This study provides evidence that the formin DIAPH3 belongs to a novel class of metastasis suppressors that inhibits conversion to an amoeboid phenotype. Inactivation of this gene appears relevant to several human malignancies, including prostate and breast carcinomas. We identified a consensus area of significant recurrent deletion on chromosome 13 encompassing the DIAPH3 locus and showed that DIAPH3 genomic loss and/or decreased DIAPH3 expression occurs in organ-confined tumours, but occurs at higher frequency in advanced disease, circulating prostate tumour cells, and metastatic lesions. We show that DIAPH3 silencing enhances tumour cell invasion, promotes amoeboid features in disparate cell backgrounds, and enhances experimental metastasis in vivo.

This is the first example of a genomic lesion affecting a direct cytoskeletal regulator that governs the amoeboid transition. Because amoeboid behaviour enables cells to squeeze through gaps in the fibrillar matrix, amoeboid cells are proposed to possess a higher proclivity to disseminate and metastasize (Sanz-Moreno & Marshall, 2010). We provide evidence that DIAPH3 deficiency promotes a wide range of amoeboid characteristics, and can cooperate with a canonical activated oncogene. In a mammary epithelial background, activated
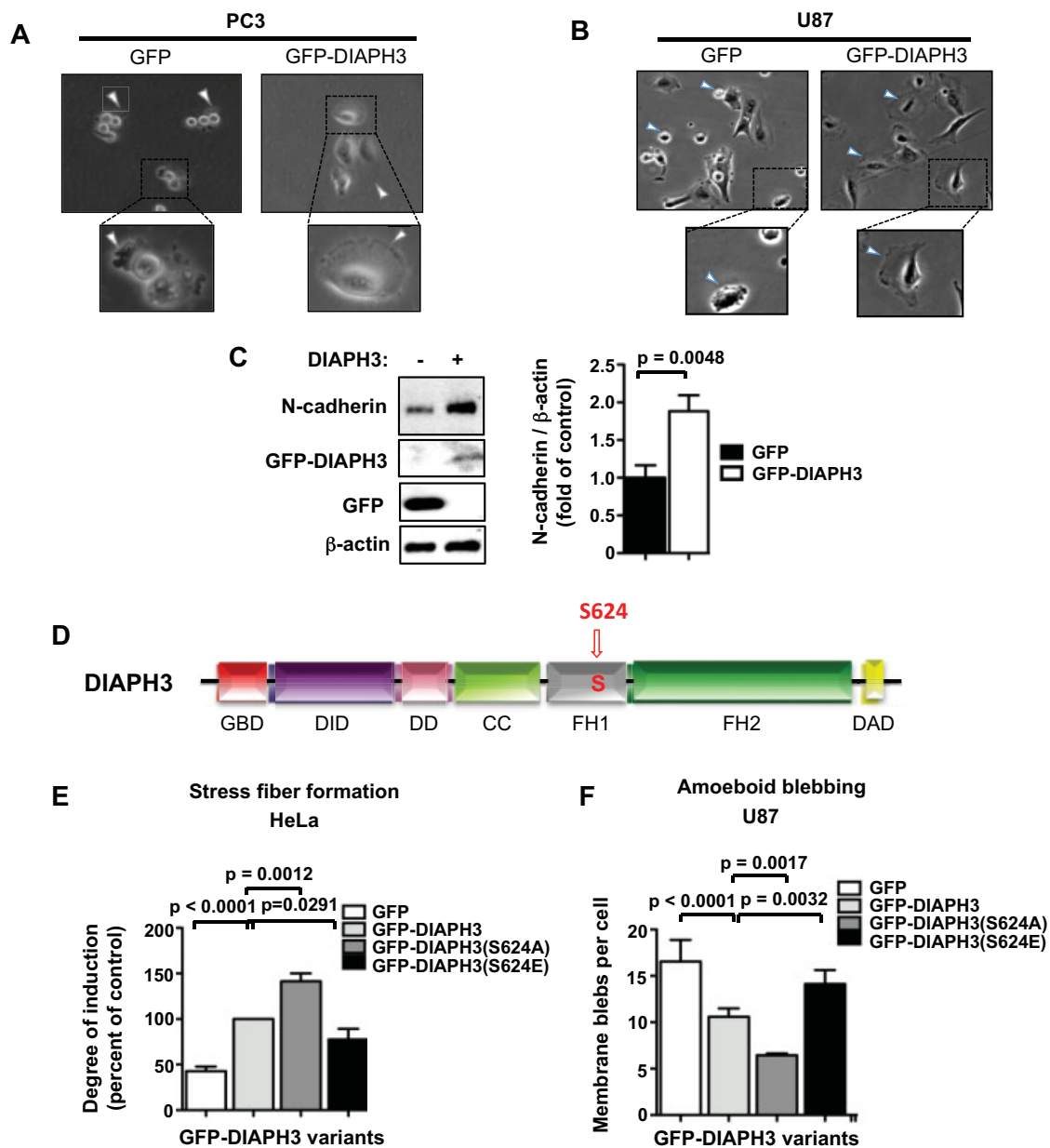
Figure 8. DIAPH3 expression suppresses the amoeboid phenotype.

A,B. Micrographs of PC3 (**A**) and U87 (**B**) cells expressing GFP or GFP-DIAPH3. Arrows indicate prevalence of amoeboid cells in PC3- or U87-GFP (left panels), and of mesenchymal (lamellopodia-enriched) cells in PC3- or U87-GFP-DIAPH3 (right panels).

C. N-cadherin is significantly upregulated in cells expressing GFP-DIAPH3.

D. Domain structure of DIAPH3 and location of the S624 phosphosite within the FH1 domain.

E. Quantitation of stress fiber formation in HeLa cells expressing GFP or DIAPH3 mutants and stained with phalloidin.

F. Quantitation of amoeboid blebbing in U87 cells expressing GFP or DIAPH3 mutants and stained with CTxB ($N \geq 2$ independent trials).

HRAS alone induced EMT; in contrast, DIAPH3 silencing in the context of activated HRAS resulted in an amoeboid transition consisting of a dramatic morphologic transformation in basement membrane cultures and high invasive potential (Fig 2). These findings suggest that the oncogenic background of tissues in which *DIAPH3* is lost makes an essential contribution to tumour behaviour.

We also showed that an endosomal trafficking defect can elicit amoeboid behaviour. We propose a model (Fig 10) whereby *DIAPH3* loss causes cytoskeletal disruption, inhibits endocytic down-regulation of RTKs, and leads to persistent activation of downstream effectors. That DIAPH3 down-regulation enhances endosomal accumulation of EGFR is notable given recent reports implicating endocytic trafficking
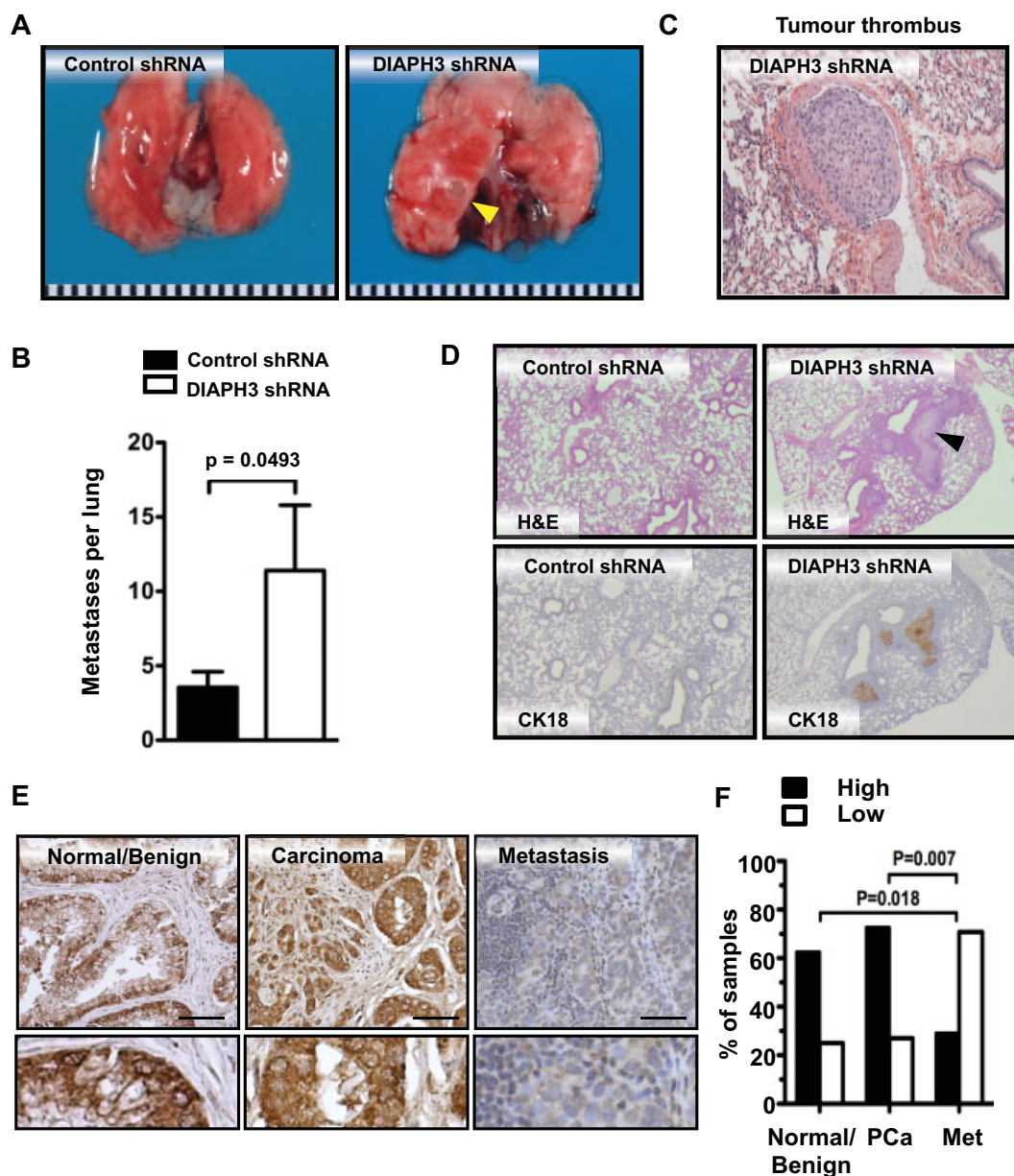
Figure 9. Silencing of DIAPH3 promotes metastasis and is associated with metastatic disease *in vivo*.

A. DIAPH3-silenced DU145 cells injected into the tail vein of nude mice produced large superficial pulmonary metastases (arrowhead).

B. Quantification of lung metastases in mice injected with control or DIAPH3-silenced DU145 cells (Mann–Whitney U test). $N = 10$ mice/condition.

C. Representative thromboembolus from lung sections from mice injected with DIAPH3-silenced DU145 cells.

D. Representative lung sections of mice injected with cells expressing control or DIAPH3 shRNAs, stained with H&E or an antibody to human CK18. Note presence of micrometastases in sections from DIAPH3 shRNA mice (arrowhead; $N = 2$ independent trials).

E. DIAPH3 IHC staining of a human tissue microarray (TMA) containing cores with benign human prostate epithelium (Normal/Benign), prostate tumour tissue (Carcinoma) and tissue from metastatic lesions (Metastasis). High-power magnifications are shown (bottom). Scale = 200 μm.

F. DIAPH3 expression is significantly decreased in metastases (Fisher's exact test, $p = 0.018/0.007$).

in tumour suppression (Mosesson et al, 2008) and demonstrating increased signalling from EGFR, VEGFR and c-MET if endosome processing is compromised (Joffre et al, 2011; Lanahan et al, 2010; Wang et al, 2009). Our findings suggest that amoeboid behaviour is a disease-relevant outcome of the ability of DIAPH3-silenced tumour cells to usurp the endocytic machinery.

Our model proposes that deregulated endosomal trafficking and signalling defects associated with DIAPH3 silencing arise from MT disruption. DIAPH3 loss induced MT instability and
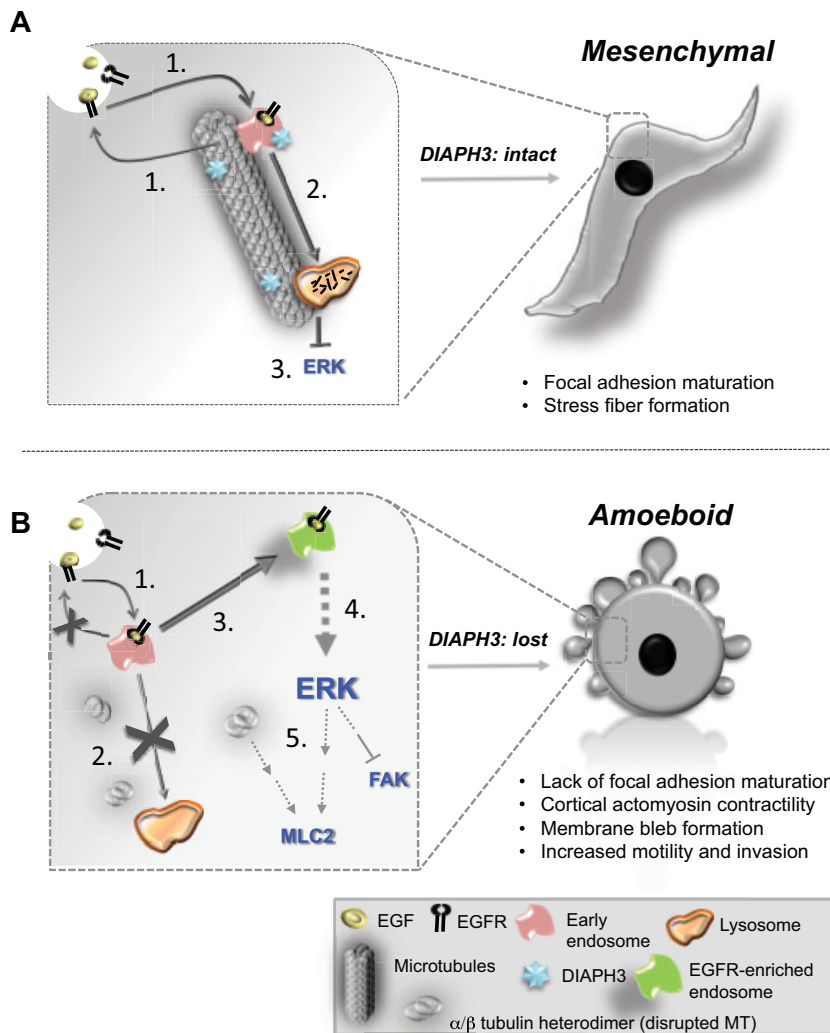
Figure 10. Model of DIAPH3 perturbation and the amoeboid transition.

A. When DIAPH3 is functional: (1) EGFR is internalized via endocytosis upon activation; (2) EGFR traffics in endosomes along microtubules to lysosomes or is recycled back to the plasma membrane; (3) ERK activity is attenuated following EGFR down-regulation.

B. When DIAPH3 is lost or inactivated: (1) EGFR is internalized. (2) MT are destabilized, preventing both transport of EGFR from early endosomes to lysosomes, and receptor recycling. (3) Active EGFR accumulates in endosomes. (4) ERK activity is sustained. (5) Deregulation of proteins promoting amoeboid characteristics (*e.g.* MLC2, FAK) evokes cortical actomyosin contraction, focal adhesion turnover, and membrane blebbing. Broken arrows/lines indicate the presence of signalling intermediates.

EGFR activation, in agreement with reports of a positive correlation between tubulin acetylation and EGFR degradation (Deribe et al, 2009; Gao et al, 2010). MT instability is emerging as a contributor to the amoeboid phenotype (Belletti et al, 2008; Berton et al, 2009). Our findings suggest that DIAPH3 is a key regulatory node in the transition between amoeboid and mesenchymal tumour cell phenotypes and that MT disruption may affect amoeboid and mesenchymal features at multiple levels.

The sustained endosomal localization of EGFR consequent to DIAPH3 downregulation may be clinically relevant. Response of a tumour cell population to a TKI can be influenced by distribution of intracellular EGFR, such that some 'sensitive' cells display EGFR on the plasma membrane while 'resistant' cells exhibit perinuclear localization (Huang et al, 2009). Alternatively, while the ligand-bound receptor undergoes normal endocytic trafficking in 'responsive' cells, transport to lysosomes can be defective in 'resistant' cells (Nishimura et al, 2007). We observed similar responses with DIAPH3 deficiency, which markedly reduced sensitivity to a TKI. Our findings are

suggestive that *DIAPH3* loss can induce resistance to EGFR inhibitors. This possibility deserves further exploration.

The RAS/MAPK axis is upregulated in 90% of metastatic PCa lesions (Taylor et al, 2010), and hyper-activation of ERK is implicated in PCa progression (Gioeli et al, 1999). However, it remains unclear how this pathway is activated, since comprehensive profiling of prostate tumours did not reveal activating mutations in BRAF or HRAS (Burger et al, 2006; Thomas et al, 2007). It is notable, then, that in PCa cells DIAPH3 deficiency upregulates ERK activity. Our results raise the interesting possibility that MEK inhibitors may be useful to target advanced disease in patients with tumours with *DIAPH3* loss.

Two recent reports assessed DIAPH3 in the context of cell invasion. Lizarraga et al. demonstrated that DIAPH3 silencing inhibits formation of filopodia-like invadopodia, invasion and degradation of 3D-matrices (Lizarraga et al, 2009). We observed DIAPH3 loss to induce a switch to an amoeboid phenotype, in which dependence on proteases for invasion is reportedly reduced (Friedl & Wolf, 2010). However, while DIAPH3 silencing suppressed invasion of MDA-MB-231 cells through

The paper explained

PROBLEM:

While metastatic disease underlies most cancer-related mortality, few genetic lesions that select for metastatic tumour cell variants have been identified. Amoeboid motility is one of several diverse modes adopted by disseminating tumour cells. Elucidation of networks and critical signaling nodes that confer or restrain the amoeboid phenotype would facilitate discovery of novel therapies to control metastasis. The *DIAPH3* locus, encoding the protein Diaphanous-related formin-3 (DIAPH3), resides at a chromosomal location that is frequently lost in metastatic prostate cancer. The potential functional significance of loss of this locus is unknown.

RESULTS:

Analysis of genome-wide, SCNA revealed that the *DIAPH3* locus was a consensus area of chromosomal deletion common to several carcinomas. *DIAPH3* deletions accumulated during disease progression, were strongly associated with metastatic disease, and were prevalent in DTCs from patient bone marrow aspirates. DIAPH3 silencing cooperated with oncogenic transformation to evoke an amoeboid phenotype in several tumour cell backgrounds. Loss of DIAPH3 caused cytoskeletal and endocytic trafficking defects through which EGFR/MEK/ERK signaling was hyperactivated. Pharmacologic inhibition of MEK suppressed the amoeboid phenotype, but tyrosine kinase inhibitors were ineffective. DIAPH3 silencing potentiated formation of pulmonary metastases *in vivo*, and its loss correlated with metastasis in human tumours.

IMPACT:

This is the first report showing that loss of a cytoskeleton remodelling protein, encoded by a locus that is lost at high frequency in multiple tumours and is strongly associated with metastasis, results in acquisition of the amoeboid cancer cell phenotype. These results may have prognostic utility to distinguish low-risk from high-risk disease.

Matrigel (Lizarraga et al, 2009), we observed DIAPH3 silencing to promote invasion through collagen I. Using an siRNA screen for formin family regulators of membrane blebbing, Stastna et al. reported that DIAPH3 silencing inhibited bleb formation and promoted cell spreading in HeLa cells (Stastna et al, 2011). Of the multiple transcripts of the *DIAPH3* locus, Isoform 1 mediated bleb formation, while an activated variant of Isoform 7 instead promoted filopodia. Consistent with the last observation, we observed a significant reduction in filopodia following *DIAPH3* silencing of HMEC-HRAS^V12 (unpublished observations). We employed Isoform 7 for our studies, however DIAPH3 silencing potentiated bleb formation, reduced adhesion and increased rates of migration in COS7, DU145 and HMEC. Although genetic heterogeneity or different characteristics of diverse ECM used in these *in vitro* studies may play a role in these diverse effects, collectively they are consistent with the conclusion that DIAPH3 resides at an important signaling node that controls invasive behaviour. Importantly, the genomic loss data and other findings from human cohorts that we present here are consistent with the conclusion that DIAPH3 inactivation is likely to promote aggressive behaviour in prostate, breast and possibly other tumour types. In the present study, we also identified a serine residue in the DIAPH3 FH1 domain that seems to result in inactivation of the protein when phosphorylated. This finding suggests that DIAPH3 might be inactivated by upstream signaling pathways in addition to gene disruption.

Reports have speculated about the presence of a tumour suppressor at 13q21 that is independent of *RB1*. A recent study evaluated somatic homozygous deletions (HDs) at high resolution in 746 cancer cell lines (Bignell et al, 2010), identifying an 'unexplained' HD cluster on chromosome 13 that exhibits a signature similar to known tumour suppressors. This cluster was separate from the dominating HD cluster affecting the *RB1* locus and had not been assigned to a known tumour suppressor gene. *DIAPH3* is a candidate non-canonical tumour suppressor in this region.

In conclusion, identification of DIAPH3 as a protein capable of mediating the switch between mesenchymal and amoeboid phenotypes provides new insight into the molecular processes of metastasis, and may facilitate design of more effective strategies against advanced disease.

MATERIALS AND METHODS

Copy number analysis

DNA copy number alterations were analysed with the Integrated Genomics Viewer using genome-wide GISTIC data (Beroukhim et al, 2007). *DIAPH3* copy number status of PCa patients was analysed using comparative genomic hybridization (cCGH) and Affymetrix Genome-Wide SNP Array data (Liu et al, 2009). The frequency of *DIAPH3* loss in circulating tumours cells was assessed using array CGH data (Holcomb et al, 2008).

Immunohistochemistry and tissue microarrays

The human prostate tissue microarray consisted of normal/benign ($n = 16$), prostate tumour ($n = 22$) and metastatic tissue cores ($n = 24$). Immunohistochemistry was performed with DIAPH3 (HNH3.1) or cytokeratin 18 antibodies.
Immunoblotting was performed as described in Supporting Information.

RNAi

For sequences and transfection methods, see Supporting Information. Multiple, independent hairpins and duplexes (>4) produced similar results in numerous readouts.

Immunofluorescence

Antibodies used: Acetylated tubulin and Rab11 (Abcam), FITC-conjugated anti-FLAG (Sigma), FITC-conjugated anti-EEA1 (BD Biosciences), EGFR (Biosource), FITC-Cholera Toxin B (CTxB, Sigma), FAK(Y397), MLC2, pMLC2(S19) and Rab5, (Cell Signaling). F-actin was detected with rhodamine-phalloidin (Invitrogen). An Axioplan 2 microscope (Zeiss) equipped with an AxioCam camera was used for fluorescence imaging.

Quantitation of EGFR-positive endosomes and focal adhesions: Duplicate slides were evaluated by three observers blinded to the experimental group in two independent experiments, in >50 cells/condition per experiment.

Tubulin acetylation: DU145 cells were incubated with acetylated tubulin antibodies, and fluorescence quantified using Axiovision 4.5 software (Zeiss). Images were rendered using ImageJ processing software. Where noted, cells were stained with rhodamine–phalloidin or FITC-CTxB prior to fixation.

Rab11 co-localization: DU145 cells were incubated with antibodies against Rab11 and EGFR, and fluorescent co-localization analysed with ImageJ. Regions with pixel intensity common to Rab11 and EGFR were highlighted.

Where indicated, cells plated on collagen I were pretreated with nocodazole (2 μM, Sigma) for 30 min, and processed as above with EGFR antibodies.

Morphogenesis assay

Three-dimensional culture of epithelial cells was performed as described (Debnath et al, 2002). Briefly, cells were seeded onto Matrigel basement membrane matrix, and acini size measured and analysed with Fiji image processing software.

Luminescence proliferation assay

Viable cells were quantified with the CellTiter-Glo assay (Promega), with luminescence measured every 24 h with a FLUOstar Omega platereader (BMG Labtech).

Experimental Metastasis Model

Animal studies were conducted in compliance with Children's Hospital Boston IACUC guidelines using BALB/c nude mice (Massachusetts General Hospital). DU145 cells expressing control or DIAPH3 shRNAs were resuspended in HBSS, injected into the tail veins of anesthetized mice (15 animals per group), and after 8 weeks mice were sacrificed, lungs isolated and each lobe fixed individually in 10% formalin.

Time-lapse video microscopy and track-plot analysis

Cell migration was monitored with an inverted microscope, collecting images every 2 min for 30 h, and movies analysed using Bioimaging software (Andor).

Real-time invasion assay

Cells labelled with CellTracker Red CMTPX (Molecular Probes) were seeded onto collagen I-coated FluoroBlok™ inserts, and fluorescence intensity of cells migrated towards chemo-attractants monitored at 6 or 12 h.

Statistical analyses

Student's *t*-test (two-tailed) was used if data were normally distributed. Otherwise, Mann–Whitney U, ANOVA, or Fisher's exact tests were used. Analyses were performed with Prism 5.0a software. Data were plotted as mean ± SD.

References

Bartolini F, Gundersen GG (2010) Formins and microtubules. Biochim Biophys Acta 1803: 164-173

Bartolini F, Moseley JB, Schmoranzer J, Cassimeris L, Goode BL, Gundersen GG (2008) The formin mDia2 stabilizes microtubules independently of its actin nucleation activity. J Cell Biol 181: 523-536

Belletti B, Nicoloso MS, Schiappacassi M, Berton S, Lovat F, Wolf K, Canzonieri V, D'Andrea S, Zucchetto A, Friedl P, et al (2008) Stathmin activity influences sarcoma cell shape, motility, and metastatic potential. Mol Biol Cell 19: 2003-2013

Beroukhim R, Getz G, Nghiemphu L, Barretina J, Hsueh T, Linhart D, Vivanco I, Lee JC, Huang JH, Alexander S, et al (2007) Assessing the significance of chromosomal aberrations in cancer: Methodology and application to glioma. Proc Natl Acad Sci USA 104: 20007-20012

Beroukhim R, Mermel CH, Porter D, Wei G, Raychaudhuri S, Donovan J, Barretina J, Boehm JS, Dobson J, Urashima M, et al (2010) The landscape of somatic copy-number alteration across human cancers. Nature 463: 899-905

Berton S, Belletti B, Wolf K, Canzonieri V, Lovat F, Vecchione A, Colombatti A, Friedl P, Baldassarre G (2009) The tumor suppressor functions of p27(kip1) include control of the mesenchymal/amoeboid transition. Mol Cell Biol 29: 5031-5045

Bignell GR, Greenman CD, Davies H, Butler AP, Edkins S, Andrews JM, Buck G, Chen L, Beare D, Latimer C, *et al* (2010) Signatures of mutation and selection in the cancer genome. Nature 463: 893-898

Burger M, Denzinger S, Hammerschmied C, Tannapfel A, Maderstorfer A, Wieland WF, Hartmann A, Stoehr R (2006) Mitogen-activated protein kinase signaling is activated in prostate tumors but not mediated by B-RAF mutations. Eur Urol 50: 1102-1109; discussion 1109–1110

Chalkia D, Nikolaidis N, Makalowski W, Klein J, Nei M (2008) Origins and evolution of the formin multigene family that is involved in the formation of actin filaments. Mol Biol Evol 25: 2717-2733

Debnath J, Mills KR, Collins NL, Reginato MJ, Muthuswamy SK, Brugge JS (2002) The role of apoptosis in creating and maintaining luminal space within normal and oncogene-expressing mammary acini. Cell 111: 29-40

Deribe YL, Wild P, Chandrashaker A, Curak J, Schmidt MH, Kalaidzidis Y, Milutinovic N, Kratchmarova I, Buerkle L, Fetchko MJ, *et al* (2009) Regulation of epidermal growth factor receptor trafficking by lysine deacetylase HDAC6. Sci Signal 2: ra84

Di Vizio D, Kim J, Hager MH, Morello M, Yang W, Lafargue CJ, True LD, Rubin MA, Adam RM, Beroukhim R, *et al* (2009) Oncosome formation in prostate cancer: Association with a region of frequent chromosomal deletion in metastatic disease. Cancer Res 69: 5601-5609

Dong JT, Chen C, Stultz BG, Isaacs JT, Frierson HF, Jr (2000) Deletion at 13q21 is associated with aggressive prostate cancers. Cancer Res 60: 3880-3883

Fernandez-Borja M, Janssen L, Verwoerd D, Hordijk P, Neefjes J (2005) RhoB regulates endosome transport by promoting actin assembly on endosomal membranes through Dia1. J Cell Sci 118: 2661-2670

Finak G, Bertos N, Pepin F, Sadekova S, Souleimanova M, Zhao H, Chen H, Omeroglu G, Meterissian S, Omeroglu A, *et al* (2008) Stromal gene expression predicts clinical outcome in breast cancer. Nat Med 14: 518-527

Friedl P, Wolf K (2010) Plasticity of cell migration: A multiscale tuning model. J Cell Biol 188: 11-19

Gaillard J, Ramabhadran V, Neumann E, Gurel P, Blanchoin L, Vantard M, Higgs HN (2011) Differential interactions of the formins INF2, mDia1, and mDia2 with microtubules. Mol Biol Cell 22: 4575-4587

Gao YS, Hubbert CC, Yao TP (2010) The microtubule-associated histone deacetylase 6 (HDAC6) regulates epidermal growth factor receptor (EGFR) endocytic trafficking and degradation. J Biol Chem 285: 11219-11226

Gasman S, Kalaidzidis Y, Zerial M (2003) RhoD regulates endosome dynamics through diaphanous-related formin and Src tyrosine kinase. Nat Cell Biol 5: 195-204

Gioeli D, Mandell JW, Petroni GR, Frierson HF, Jr, Weber MJ (1999) Activation of mitogen-activated protein kinase associated with prostate cancer progression. Cancer Res 59: 279-284

Goode BL, Eck MJ (2007) Mechanism and function of formins in the control of actin assembly. Annu Rev Biochem 76: 593-627

Hamadi A, Bouali M, Dontenwill M, Stoeckel H, Takeda K, Ronde P (2005) Regulation of focal adhesion dynamics and disassembly by phosphorylation of FAK at tyrosine 397. J Cell Sci 118: 4415-4425

Holcomb IN, Grove DI, Kinnunen M, Friedman CL, Gallaher IS, Morgan TM, Sather CL, Delrow JJ, Nelson PS, Lange PH, *et al* (2008) Genomic alterations indicate tumor origin and varied metastatic potential of disseminated cells from prostate cancer patients. Cancer Res 68: 5599-5608

Hosoki S, Ota S, Ichikawa Y, Suzuki H, Ueda T, Naya Y, Akakura K, Igarashi T, Oshimura M, Nihei N, *et al* (2002) Suppression of metastasis of rat prostate cancer by introduction of human chromosome 13. Asian J Androl 4: 131-136

Huang DH, Su L, Peng XH, Zhang H, Khuri FR, Shin DM, Chen ZG (2009) Quantum dot-based quantification revealed differences in subcellular localization of EGFR and E-cadherin between EGFR-TKI sensitive and insensitive cancer cells. Nanotechnology 20: 225102

Joffre C, Barrow R, Menard L, Calleja V, Hart IR, Kermorgant S (2011) A direct role for Met endocytosis in tumorigenesis. Nat Cell Biol 13: 827-837

Kainu T, Juo SH, Desper R, Schaffer AA, Gillanders E, Rozenblum E, Freas-Lutz D, Weaver D, Stephan D, Bailey-Wilson J, *et al* (2000) Somatic deletions in hereditary breast cancers implicate 13q21 as a putative novel breast cancer susceptibility locus. Proc Natl Acad Sci USA 97: 9603-9608

Kalluri R, Weinberg RA (2009) The basics of epithelial–mesenchymal transition. J Clin Invest 119: 1420-1428

Lanahan AA, Hermans K, Claes F, Kerley-Hamilton JS, Zhuang ZW, Giordano FJ, Carmeliet P, Simons M (2010) VEGF receptor 2 endocytic trafficking regulates arterial morphogenesis. Dev Cell 18: 713-724

Li HR, Wang-Rodriguez J, Nair TM, Yeakley JM, Kwon YS, Bibikova M, Zheng C, Zhou L, Zhang K, Downs T *et al* (2006) Two-dimensional transcriptome profiling: Identification of messenger RNA isoform signatures in prostate cancer from archived paraffin-embedded cancer specimens. Cancer Res 66: 4079-4088

Liu W, Laitinen S, Khan S, Vihinen M, Kowalski J, Yu G, Chen L, Ewing CM, Eisenberger MA, Carducci MA, *et al* (2009) Copy number analysis indicates monoclonal origin of lethal metastatic prostate cancer. Nat Med 15: 559-565

Lizarraga F, Poincloux R, Romao M, Montagnac G, Le Dez G, Bonne I, Rigaill G, Raposo G, Chavrier P (2009) Diaphanous-related formins are required for invadopodia formation and invasion of breast tumor cells. Cancer Res 69: 2792-2800

Mas VR, Maluf DG, Archer KJ, Yanek K, Kong X, Kulik L, Freise CE, Olthoff KM, Ghobrial RM, McIver P, *et al* (2009) Genes involved in viral carcinogenesis and tumor initiation in hepatitis C virus-induced hepatocellular carcinoma. Mol Med 15: 85-94

Mosesson Y, Mills GB, Yarden Y (2008) Derailed endocytosis: An emerging feature of cancer. Nat Rev Cancer 8: 835-850

Nishimura Y, Bereczky B, Ono M (2007) The EGFR inhibitor gefitinib suppresses ligand-stimulated endocytosis of EGFR via the early/late endocytic pathway in non-small cell lung cancer cell lines. Histochem Cell Biol 127: 541-553

Peng J, Wallar BJ, Flanders A, Swiatek PJ, Alberts AS (2003) Disruption of the Diaphanous-related formin Drf1 gene encoding mDia1 reveals a role for Drf3 as an effector for Cdc42. Curr Biol 13: 534-545

Pinner S, Sahai E (2008) PDK1 regulates cancer cell motility by antagonising inhibition of ROCK1 by RhoE. Nat Cell Biol 10: 127-137

Sahai E, Marshall CJ (2003) Differing modes of tumour cell invasion have distinct requirements for Rho/ROCK signalling and extracellular proteolysis. Nat Cell Biol 5: 711-719

Sanz-Moreno V, Gadea G, Ahn J, Paterson H, Marra P, Pinner S, Sahai E, Marshall CJ (2008) Rac activation and inactivation control plasticity of tumor cell movement. Cell 135: 510-523

Sanz-Moreno V, Marshall CJ (2010) The plasticity of cytoskeletal dynamics underlying neoplastic cell migration. Curr Opin Cell Biol 22: 690-696

Schmidt S, Friedl P (2010) Interstitial cell migration: Integrin-dependent and alternative adhesion mechanisms. Cell Tissue Res 339: 83-92

Soldati T, Schliwa M (2006) Powering membrane traffic in endocytosis and recycling. Nat Rev Mol Cell Biol 7: 897-908

Sonee M, Barron E, Yarber FA, Hamm-Alvarez SF (1998) Taxol inhibits endosomal–lysosomal membrane trafficking at two distinct steps in CV-1 cells. Am J Physiol 275: C1630-C1639

Sorkin A, von Zastrow M (2009) Endocytosis and signalling: Intertwining molecular networks. Nat Rev Mol Cell Biol 10: 609-622

Stastna J, Pan X, Wang H, Kollmannsperger A, Kutscheidt S, Lohmann V, Grosse R, Fackler OT (2011) Differing and isoform-specific roles for the formin DIAPH3 in plasma membrane blebbing and filopodia formation. Cell Res 22: 728-745

Taylor BS, Schultz N, Hieronymus H, Gopalan A, Xiao Y, Carver BS, Arora VK, Kaushik P, Cerami E, Reva B, *et al* (2010) Integrative genomic profiling of human prostate cancer. Cancer Cell 18: 11-22

Thomas RK, Baker AC, Debiasi RM, Winckler W, Laframboise T, Lin WM, Wang M, Feng W, Zander T, MacConaill L, *et al* (2007) High-throughput oncogene mutation profiling in human cancer. Nat Genet 39: 347-351

Verhey KJ, Gaertig J (2007) The tubulin code. Cell Cycle 6: 2152-2160

Wallar BJ, Deward AD, Resau JH, Alberts AS (2007) RhoB and the mammalian Diaphanous-related formin mDia2 in endosome trafficking. Exp Cell Res 313: 560-571

Wang Y, Roche O, Yan MS, Finak G, Evans AJ, Metcalf JL, Hast BE, Hanna SC, Wondergem B, Furge KA, et al (2009) Regulation of endocytosis via the oxygen-sensing pathway. Nat Med 15: 319-324

Wikman H, Vessella R, Pantel K (2008) Cancer micrometastasis and tumour dormancy. Apmis 116: 754-770

Wolf K, Mazo I, Leung H, Engelke K, von Andrian UH, Deryugina EI, Strongin AY, Brocker EB, Friedl P (2003) Compensation mechanism in tumor cell migration: Mesenchymal–amoeboid transition after blocking of pericellular proteolysis. J Cell Biol 160: 267-277

Wyckoff JB, Pinner SE, Gschmeissner S, Condeelis JS, Sahai E (2006) ROCK- and myosin-dependent matrix deformation enables protease-independent tumor–cell invasion in vivo. Curr Biol 16: 1515-1523